frontiers in Energy Research

ORIGINAL RESEARCH
published: 30 April 2018
doi: 10.3389/fenrg.2018.00018

Microwave-Assisted Coprecipitation Synthesis of $LaCoO_3$ Nanoparticles and Their Catalytic Activity for Syngas Production by Partial Oxidation of Methane

Consuelo Alvarez-Galvan[1], Annette Trunschke[2], Horacio Falcon[1†], Maricruz Sanchez-Sanchez[2†], Jose Miguel Campos-Martin[1], Robert Schlögl[2] and Jose Luis G. Fierro[1]*

[1] Instituto de Catálisis y Petroleoquímica (CSIC) Cantoblanco, Madrid, Spain, [2] Department of Inorganic Chemistry, Fritz-Haber-Institut (Max-Planck-Gesellschaft), Berlin, Germany

OPEN ACCESS

Edited by:
Luis M. Gandía, Universidad Pública de Navarra, Spain

Reviewed by:
Maria A. Goula, Western Macedonia University of Applied Science, Greece
Fabio Barboza Passos, Federal Fluminense University, Brazil
Jordi Llorca, Universitat Politecnica de Catalunya, Spain

***Correspondence:**
Consuelo Alvarez-Galvan
c.alvarez@icp.csic.es

†Present address:
Horacio Falcon, Centro de Investigaciones en Nanociencia y Nanotecnología (NANOTEC), UTN-Facultad Regional Córdoba, Córdoba, Argentina;
Maricruz Sanchez-Sanchez, Department of Chemistry and Catalysis Research Center, Technische Universität München, Garching, Germany

Specialty section:
This article was submitted to Advanced Fossil Fuel Technologies, a section of the journal Frontiers in Energy Research

Received: 12 January 2018
Accepted: 05 March 2018
Published: 30 April 2018

Citation:
Alvarez-Galvan C, Trunschke A, Falcon H, Sanchez-Sanchez M, Campos-Martin JM, Schlögl R and Fierro JLG (2018) Microwave-Assisted Coprecipitation Synthesis of $LaCoO_3$ Nanoparticles and Their Catalytic Activity for Syngas Production by Partial Oxidation of Methane. Front. Energy Res. 6:18. doi: 10.3389/fenrg.2018.00018

$LaCoO_3$ perovskite-type oxides were prepared by microwave-assisted coprecipitation route and investigated in the catalytic partial oxidation of methane (CPOM) to syngas. This preparation method aims to achieve higher specific surface areas (ssa) than soft-chemical methods commonly used in the preparation of engineered materials. In an attempt to accomplish the creation of mesostructured porous $LaCoO_3$, an ionic template such as cetyl trimethyl ammonium bromide has been used as endotemplate in some samples. The influence of pH and the type of precipitating agent has been studied. The materials have been characterized at different levels: morphology has been studied by scanning electron microscopy, textural properties by nitrogen adsorption–desorption at −196°C, structural analysis by X-ray diffraction, surface composition by X-ray photoelectron spectroscopy, thermal stability by thermogravimetric analysis, and carbon formation in spent catalysts by Raman spectroscopy. Structure-activity correlations point out that the precipitating agent has a key role on the morphology and porosity of the resultant oxide, as well as on the average crystalline domain of lanthanum perovskite (catalyst precursor). Thus, the use of ammonium hydroxide as precipitant leads to materials with a higher surface area and a greater ssa of cobalt (per unit mass), improving their catalytic performance for the CPOM reaction. The best catalytic performance was found for the catalyst prepared using ammonium hydroxide as precipitant (pH 9) and without adding CTAB as endotemplate.

Keywords: methane, partial oxidation, syngas, microwave-assisted coprecipitation, endotemplate

INTRODUCTION

Natural gas is found in many locations around the world (more distributed than oil reserves) and avoids dependence from oil producing countries. However, the low cost of oil coupled with the high cost of natural gas storage and transportation from remote reservoirs hampers its use. At present, numerous efforts have been done investigating on methods to enhance the value of natural gas, either by synthesizing chemicals or fuels or more readily transportable products that nowadays are mainly obtained by crude oil refining. Currently, the only economically available route for the conversion

of methane into more valuable chemicals is *via* synthesis gas. Among the different routes for syngas production from methane (steam reforming, dry reforming, and partial oxidation), partial oxidation presents some advantages: it is a mild exothermic reaction, leading to energy saving, therefore, it offers economic incentives when compared to the current industrial process, based on the steam reforming which is a very endothermic reaction. Moreover, catalytic partial oxidation of methane (CPOM) produces a H_2/CO ratio ~2 (suitable for Fischer–Tropsch or methanol syntheses). The main drawbacks are the formation of hotspots in the catalytic bed (which favors the sintering of the active phase), carbon formation and, in some cases, the need of an oxygen separation plant (York, 2003).

Metallic cobalt supported on basic oxide supports proved to be efficient catalysts for syngas production by CPOM (Wang and Ruckenstein, 2001). Perovskite-type (ABO_3) oxides are excellent precursors for supported metal catalysts because, their reduction leads to finely dispersed metallic particles (B^0) onto a matrix constituted by a metal oxide (A_2O_3) (Hayakawa et al., 1993). $LaCoO_3$ is particularly promising as catalyst for reactions such as combustion or total oxidation of VOCs (Alvarez-Galvan et al., 2009) or as a catalyst precursor for syngas production by oxidative reforming of diesel (Navarro et al., 2007; Mota et al., 2012), methane reforming, and/or partial oxidation (Zhu et al., 2004; Toniolo et al., 2012; Brackmann et al., 2014; Roseno et al., 2016). However, conventional preparation routes of perovskite type oxides such as coprecipitation and sol-gel methods results in bulk materials with very low specific surface area (ssa), which limits the surface accessibility of active phases. The use of porous catalysts having a high surface area is highly desired because activity is enhanced when referred to unit mass of catalyst.

The potential of well-ordered mesoporous silica for applications in catalysis was recognized in the early 90s of the twentieth century (Kresge et al., 1992) and it has inspired numerous efforts in synthesis of non-silica-based materials composed of catalytically relevant transition metal oxides. The introduction of internal porosity in oxides, such as perovskites, is of great interest for the fields of catalysis, fuel cells, and sensors. The use of porous oxides in catalysis will increase the conversion rate per mass of catalyst and, additionally, might lead to improved selectivity as compared to the respective bulk materials, due to effects such as site isolation, which may open alternative reaction pathways. Moreover, the creation of an internal and stable porous structure would increase heat and mass diffusion, increasing the catalyst stability, by decreasing deactivation by sintering and carbon deposition.

Therefore, it is very important to stablish of a synthesis method that would lead to an increase in the dispersion of active phases. Different methods to achieve this objective involve the use of different compounds as templates or structure directing agents (ionic and neutral surfactants), in order to introduce porosity (Schuth, 2001; He and Antonelli, 2002; Soler-Illia et al., 2002; Carreon and Guliants, 2005; Taguchi and Schüth, 2005; Pal and Bhaumik, 2013). Some thermally stable binary and mixed transition metal oxides, such as $SmFe_{1-X}Al_XO_3$ (Stathopoulos et al., 2001), $Pb(Sc_{1/2}Nb_{1/2})O_3$ (Tang et al., 2009), $LaCoO_3$ (Xintong et al., 2016), La-Co-Zr-O mixed oxide (Zou et al., 2006), and $LaMnO_3$ (Hu et al., 2017) were prepared from metal salts precursors in the presence of ionic molecules such as hexadecyltrimethylammonium bromide (CTAB) as endotemplate. The main requirements of this synthesis procedure are (i) the need of interactions between the template molecule and the material precursors (Coulomb interaction, hydrogen bridges, van der Waals forces, etc.) and (ii) the difference between the density of the precursors and the template cannot be too large. The high redox activity of transition metal oxides often lead to a collapse of the mesophase during the template removal by calcination or to an incomplete elimination of the template. Thus, despite many efforts, an efficient preparation of mesoporous mixed oxides has not been reported in literature, and often, the materials prepared by such route show a collapsed structure and/or no mesoporosity (Schüth, 2003). However, the synthesis of porous perovskites using endotemplates has not been sufficiently explored.

On the other hand, another approach to develop new fast and energy-efficient routes for the synthesis of solids is the microwave-assisted method. Microwave synthesis is generally fast, simpler, and very energy efficient. Microwave interaction with reactants during the synthesis of materials is based on energy transfer from microwaves to the material through resonance or relaxation, which results in rapid heating (Rao et al., 1999). Microwave-assisted hydrothermal syntheses have been successfully used to prepare different materials, such as Ir oxohydroxides for electrochemical oxidation of water (Massué et al., 2017), $LaNiO_3$ for the electrocatalytic activity toward hydrogen evolution reaction, with a smaller grain size than non microwave-assisted routes (Galal et al., 2011), and also to achieve a uniform deposition of Pt nanoparticles on ceramic monoliths (Zavyalova et al., 2009).

This work describes an attempt of preparing $LaCoO_3$ by microwave-assisted hydrothermal synthesis, with the aid of an ionic endotemplate. The synthesis protocol aims to obtain porous materials of higher ssa and thus of enhanced catalytic activity. CTAB is a cationic surfactant, soluble in H_2O, which was introduced to interact with the nitrate salts of the corresponding cations and to improve the homogeneity of the precursors. The physicochemical properties of the materials were investigated by means of N_2 adsorption–desorption isotherms at −196°C, powder X-ray diffraction (XRD), scanning electron microscopy (SEM), X-ray photoelectron spectroscopy (XPS), and Raman spectroscopy. The prepared samples were used as catalysts precursors for syngas production by partial oxidation of methane. Correlations of structure–activity were stablished with the aim to understand which parameters are influencing the reactivity.

MATERIALS AND METHODS

Samples Preparation

In order to prepare 5 g of $LaCoO_3$, the corresponding stoichiometric amounts of cobalt and lanthanum nitrate precursors were dissolved in 100 ml bidistilled water. In the case of using CTAB as endotemplate [molar ratio CTAB/(Co + La cations)], this is suspended in water and added to the Co and La solution under stirring. The resultant gel is stirred for 30 min at 60°C. NH_4OH or NaOH is added until the pH is 9 or 11 (the color of the suspension can have different tonalities between pink and purple). Then,

the hydrothermal treatment is carried out, transferring the gel into a teflon-lined microwaved-assisted autoclave. After 4 h at 200°C, the product is filtered, washed twice with 100 ml of water to remove nitrates, and dried 14 h at 80°C. Finally, the materials were calcined under flowing air, first at 300°C for 2 h and then at 750°C for 4 h (2°C/min), obtaining black samples.

As previously commented, CTAB was used as endotemplate, for crystal growth agent. CTAB is a cationic surfactant, with a hydrophilic head and a hydrophobic organic tail. In the synthesis of the samples, $La(NO_3)_3$ and $Co(NO_3)_2$ were combined with NaOH or NH_4OH to generate hydroxide ions. Therefore, ion pairs between the hydroxide and CTA^+ were formed because of the electrostatic interaction in the alkaline solution. The hydrophilic head of CTAB is adsorbed on the surface of the nuclei of La and Co hydroxides precipitate. When the hydrothermal temperature was increased to 200°C, CTAB micelles were destroyed (Hu et al., 2017). The nomenclature of the samples is composed by the precipitant cation symbol followed by the value of the pH of precipitation and, finally, in the case of using CTAB as endotemplate, the letter "E" as suffix.

Samples Characterization

Specific surface areas were calculated using the BET method from the nitrogen adsorption isotherms recorded at −196°C using a Micromeritics ASAP 2420 automatic instrument. The accuracy of ssa values is below 0.5%. The calculation of the pore size distribution was performed using the desorption branch of the isotherm and the Barrett–Joyner–Halenda model.

The phase identification was performed by XRD analysis using an X'Pert Pro PANalytical equipment. XRD patterns were recorded using a CuKα radiation (λ = 1.5406 Å, 45 kV, 40 mA). The mean crystallite size was then estimated from X-ray line broadening using the Scherrer equation. Width was taken as the full width at half maximum intensity of the most intense and least overlapped peaks of $LaCoO_3$ (2·θ ~47.5°) for the fresh calcined samples and of Co^0 and $La(OH)_3$ (2·θ ~44.2 and 39.5°, respectively) for the catalysts after reaction.

The morphology of the fresh calcined samples was analyzed by SEM (Hitachi S-3000N), instrument with a resolution of 3 nm. The acceleration voltage was 20 kV. The samples were dispersed on aluminum stubs.

X-ray photoelectron spectroscopy measurements were recorded using an Escalab 200 R spectrometer equipped with a hemispherical electron analyzer and an Al Kα (h·ν = 1,486.6 eV) 120 W X-ray source. The area of the peaks was estimated by calculating the integral of each peak after smoothing and subtraction of an S-shaped background and fitting of the experimental curve to a mixture of Lorentzian and Gaussian lines (90G/10L). All binding energies (BE) were referenced to the C 1 s signal at 284.8 eV from carbon contamination of the samples to correct the charging effects. This reference gave BE values within an accuracy of ±0.2 eV. Quantification of the atomic fractions on the sample surface was obtained by integration of the peaks normalized with atomic sensitivity factors.

The amount of adsorbed compounds as well as the decomposition of perovskite samples during pretreatment were determined by thermogravimetric analysis (TGA/SDTA 851e Mettler Toledo), measuring the weight change of the calcined samples during heating at high temperature. Analyses were carried out by raising the sample temperature from room temperature to 950°C at a rate of 20°C/min in a N_2 flow.

Raman spectra were recorded with a Renishaw in *via* Raman Microscope spectrometer equipped with a laser beam emitting at 532 nm, at 100 mW output power. The photons scattered by the sample were dispersed by a 1,200 lines/mm grating monochromator and simultaneously collected on a CCD camera; the collection optic was set at 50× objective. These measurement conditions gave Raman shift within an accuracy lower of 0.1/cm.

Catalytic Activity Tests Protocol

The catalytic behavior of prepared samples for the partial oxidation of methane to syngas was studied under atmospheric pressure, at 900°C using a quartz fixed bed reactor (external diameter = 6 mm, internal diameter = 4 mm). The catalysts (40 mg) were subjected to a pretreatment under 44.4 mL_N/min (10% H_2–90%N_2) flow, increasing the temperature up to 900°C and maintaining these conditions for 30 min (ramp, 30°C/min). Once the activation stage has finished, the reactants are introduced. The space velocity was 36,600 mL_N/h·g and the feed composition was 40% CH_4, 20% O_2, and 40% N_2 (molar). The reaction stream was analyzed on line by gas chromatography (HP 6890), equipped with a column Carboxen 1010 PLOT (SUPELCO®) and with a thermal conductivity detector. This system was used to analyze H_2, O_2, N_2, CO, CO_2, and CH_4. Nitrogen was used as an inert standard for quantification. During the activity tests, carbon balances were always close to 100%. All reaction experiments were repeated three times with variation of the conversion and selectivity lower than two units of calculated percentage (average values are reported).

RESULTS AND DISCUSSION

Characterization of Fresh Calcined Samples

The fresh calcined samples have been analyzed by adsorption–desorption of N_2. Obtained results (BET surface area, external and micropore area, and pore volume) are reported in **Table 1**. The surface areas of this novel mesostructured $LaCoO_3$ oxide are higher than those obtained for standard $LaCoO_3$ samples, prepared by coprecipitation or sol-gel methods (Villoria et al., 2011). The samples prepared using NaOH as precipitant agent show lower ssa than those prepared using NH_4OH, under the

TABLE 1 | Textural properties of fresh calcined samples.

Catalyst	A_{BET} (m^2/g)	External surface area (m^2/g)	Micropore area (m^2/g)	Pore volume (cm^3/g)
NH4–9	16.0	14.6	1.4	0.0897
NH4–9-E	16.0	15.3	0.7	0.0648
NH4–11	16.8	15.7	1.1	0.0536
NH4–11-E	18.7	18.7	0	0.0685
Na-11	8.0	7.9	0.1	0.0292
Na-11-E	8.3	7.8	0.5	0.0164

same precipitation pH. For the samples prepared with NH_4OH, an increase of the precipitation pH from 9 to 11 produces a small increase in ssa values. Furthermore, external surface area values are somewhat higher when CTAB is incorporated to the precipitation medium. This effect is attributed to the development of a larger mesoporosity (Hellgardt and Chadwick, 1998), as it is observed when pore size distributions are compared (**Figure 1**).

Figure 2 shows the nitrogen adsorption–desorption isotherms for the fresh calcined samples. All of them are type IV isotherms, characteristic of mesoporous materials. Except for the sample Na-11-E, all the materials show, to a greater or lesser extent, a H3 hysteresis loop, due to capillary condensation in mesoporous solids containing aggregates of plate-like particles giving rise to slit-shaped pores. H3 type hysteresis loop indicates that the samples contain interparticular pores and have lost the possible inner mesoporosity introduced by CTAB, probably due to the high temperature used during the calcination (Zou et al., 2008). The N_2 adsorption/desorption isotherms of the samples show a sharp capillary condensation step at high relative pressures ($P/P_0 \sim 0.9–1.0$), indicating a relatively large pore size and wide pore distribution (Zou et al., 2008; Zhao et al., 2010).

It can be observed that, only for the sample prepared at pH 11 and using ammonium hydroxide as precipitant, an increase in mesoporosity and ssa is generated when CTAB is used as endotemplate (sample NH4–11-E in relation to NH4–11), as it was expected by the endotemplate removal (see **Figures 1** and **2**).

A very broad pore size distribution in the range of meso and macropores with a relative maximum around 60 nm has been observed for all the materials, except for the sample Na-11-E (**Figure 1**). A relative maximum around 2–3 nm is also observed for all the samples.

The crystalline composition of the samples after calcination has been determined by XRD. The diffractograms, in **Figure 3**, show that samples Na-11 and Na-11-E, prepared using NaOH to precipitate cobalt and lanthanum cations, consist only of rhombohedral lanthanum cobaltite (PDF card: 01-084-0848), characterized by the typical doublet around 32.9 and 33.3°. On the contrary, the samples prepared using NH_4OH as precipitant contain, besides of $LaCoO_3$, some other phases, such as hexagonal La_2O_3 (01-083-1344) and cubic Co_3O_4 (01-076-1802), for those named NH4–9, NH4–9-E, and NH4–11, and hexagonal $La(OH)_3$ (as well as Co_3O_4 and $LaCoO_3$) in the case of the sample NH4–11-E. The average domain size of lanthanum cobaltite has been determined using the Scherrer equation (**Table 2**). The results clearly show that the average domain size of this phase is larger for the samples synthesized using NaOH as precipitant (Na-11 and Na-11-E).

The morphology of the samples (fresh calcined) has been studied by SEM. Micrographs, in **Figure 4**, revealed some

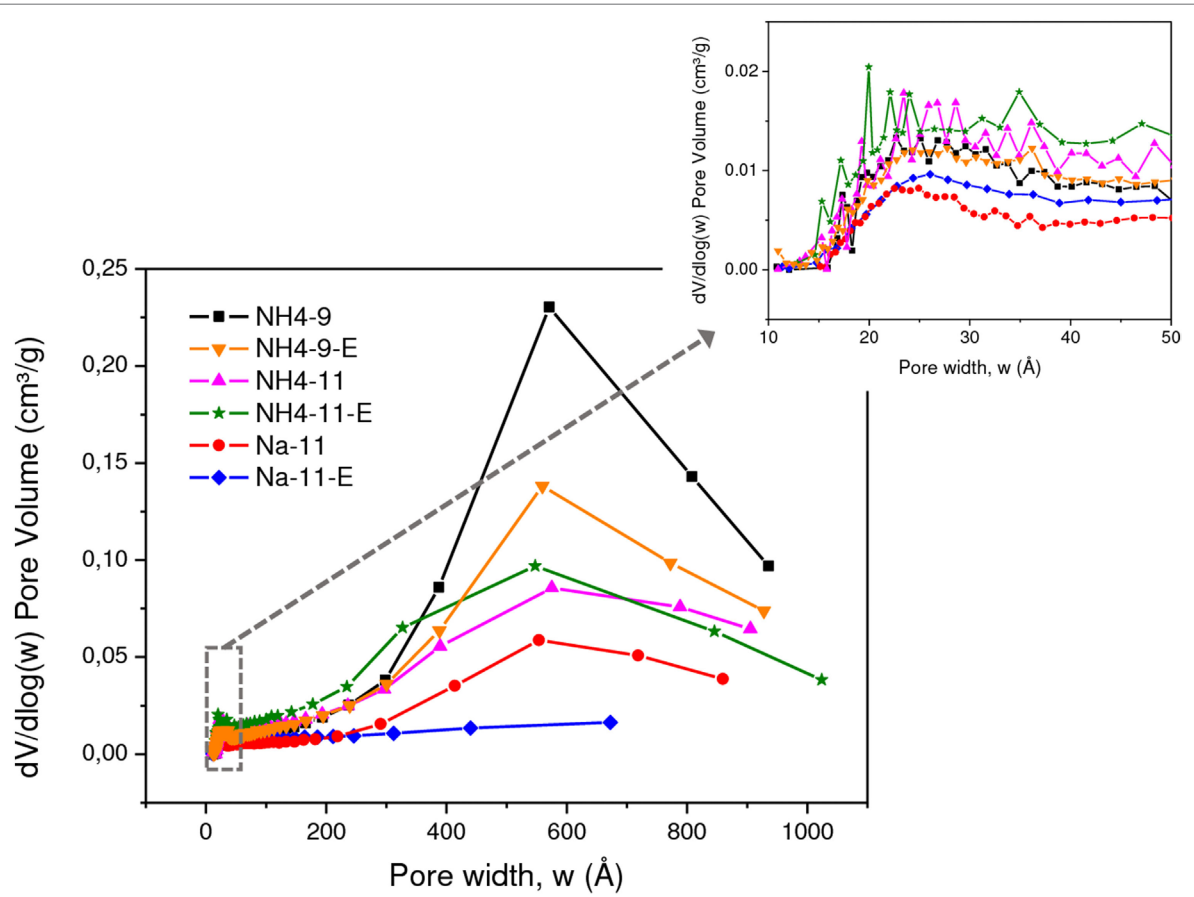

FIGURE 1 | Pore size distributions of fresh calcined samples (from Barrett–Joyner–Halenda model desorption branch).

differences depending on the preparation of the sample. In general, the particles have a granular shape, but the size and specific morphology is different. Those samples prepared using NaOH as precipitant (Na-11 and Na-11-E) show an average grain size somewhat higher (around 0.10–0.15 μm) than those prepared using NH_4OH (with an average grain size around 0.03–0.05 μm). The sample Na-11-E shows grains that are bigger, more defined and with a more regular shape than grains in Na-11 sample. In the case of the samples prepared under the same pH (11) but using ammonium hydroxide as precipitant (NH4–11 and NH4–11-E), similarly to samples prepared with NaOH, the use of an endotemplate produces more regularly shaped grains. On the other hand, the sample NH4–9 presents a nanorod-based morphology. Considering the grain size and shape observed by SEM, it can be derived that there is a correlation between these properties and the ssa (**Table 1**). In essence, a smaller grain size and more intricate morphology are related to a higher surface area. The decrease in the grain size for the samples prepared using NH_4OH was attributed to the combined effect of surfactant CTAB and precipitant ammonium hydroxide. In the samples prepared in this work, it is observed that the surfactant CTAB, which was introduced into the precipitation system to control the aggregation of precipitates, reduces the aggregation tendency of the precipitates due to its micellar effect and steric repulsive effects. Hence, in highly basic media metal hydroxo species, e.g., $(Co(OH)_4)^{2-}$, $(La(OH)_4)^{-}$, interact with the cationic template. In this way, the anionic inorganic species are stabilized with a cationic surfactant (CTA^+) through electrostatic interaction (Pal and Bhaumik, 2013).

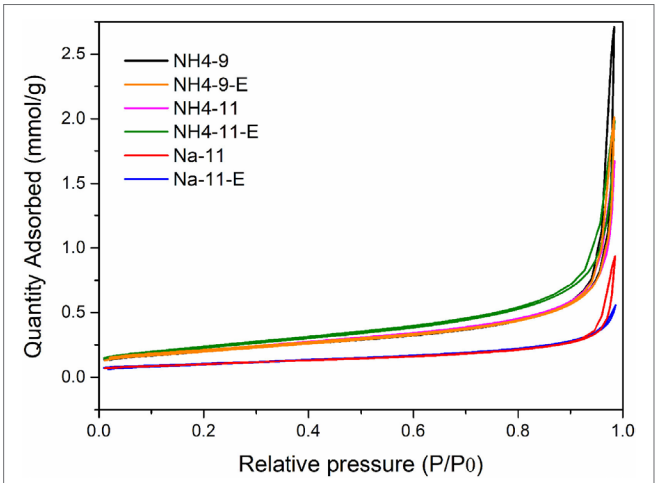

FIGURE 2 | N_2 adsorption–desorption isotherms at −196°C of fresh calcined samples.

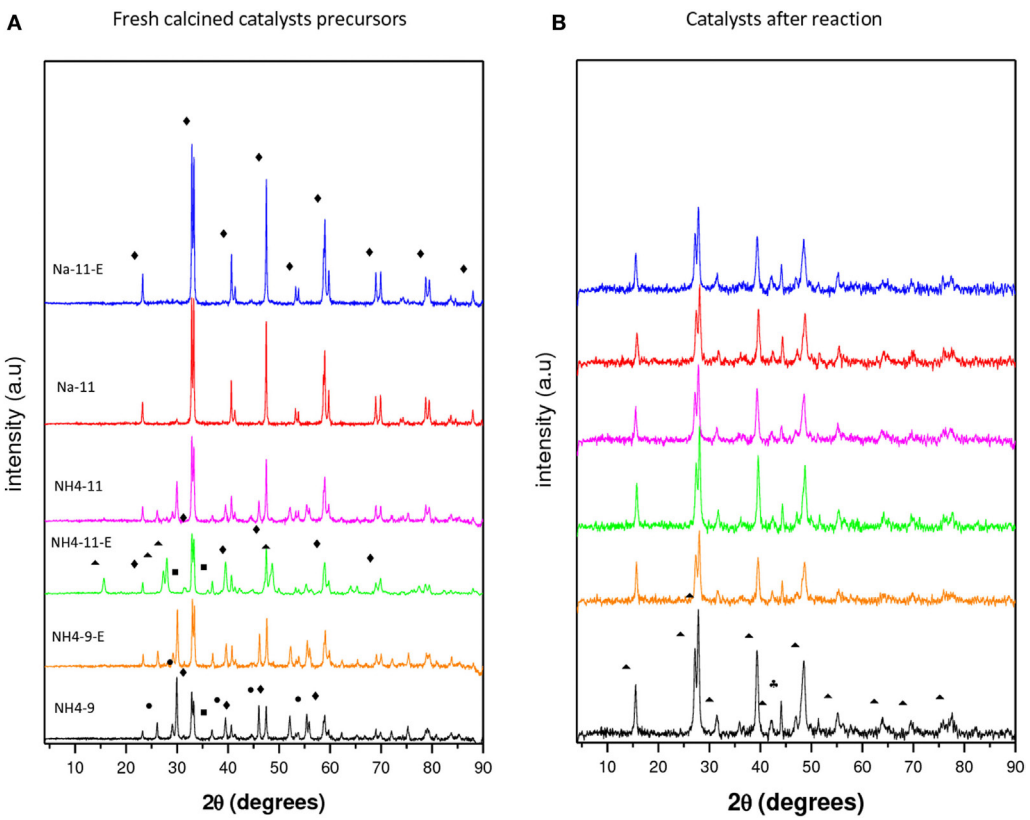

FIGURE 3 | X-ray diffractograms of **(A)** fresh calcined samples and **(B)** catalysts after reaction (♦: rhombohedral $LaCoO_3$, ■: cubic Co_3O_4, •: hexagonal La_2O_3, 5:▲ hexagonal $La(OH)_3$, ♣: Co^0).

In order to explain the role of ammonium hydroxide in decreasing the growth of the as-precipitated grains, it is necessary to comment on the formation mechanism of precipitates. The precipitation process is based on a simple reaction between metallic cations and OH^- anions to form hydroxide precipitates. Afterward, these initial precipitate particles will grow *via* a ripening process according to crystal growth theory. Ammonium cations adsorb on the nuclei and inhibit further growth of the particles due to its spatial configuration. NH_4^+ is more prone to adsorb onto the electronegative surface of the $LaCoO_3$ particles because it is a stronger Lewis acid than Na^+. Moreover, the larger size of ammonium cation increases the thickness of the electric layer on the precipitates. Consequently, the mobility of the metal ions on the surface of the particles is remarkably reduced and consequently their growth *via* Ostwald ripening is restrained (Tang et al., 2009).

These morphological properties obtained by SEM are in good agreement with results obtained by N_2 adsorption–desorption at −196°C, where the prepared solids were found to be conformed by a meso and macroporosity network. The primary lanthanum cobaltite particles are arranged into 30–150 nm agglomerates, generating mesopores of 2–50 nm diameter. These agglomerates coalesce into aggregates, and pores >50 nm are formed in the interstices (Soboleva et al., 2010).

The fresh calcined samples have been analyzed by TGA under N_2 flow and obtained profiles are depicted in **Figure 5**. The first weight loss region up to 200°C is related to loss of adsorbed water. The second one is due to the decomposition of surface lanthana carbonated hydroxide, which produces carbon dioxide and water, up to 470°C. Then, a third loss, up to 600°C is related to the decomposition of lanthanum hydroxide (Ino et al., 1976), which is evident for the sample NH4–11-E [in accordance to the presence of $La(OH)_3$, observed by XRD]. Finally, the last loss, between 600 and 830°C, is related to the formation of O_2 by solid state reaction between Co_3O_4 and La_2O_3 to form $LaCoO_3$ and by the desorption of mobile bulk oxygen associated with a defective perovskite structure (Navarro et al., 2007; Singha et al., 2017).

As reported in literature (Singha et al., 2017), the loss of CTAB is produced between 300 and 600°C, therefore, this compound was removed during the calcination stage (at 750°C), carried out in the last stage of the samples preparation (see Samples Preparation) and, because of this, none of the weight losses are attributed to the removal of this compound.

TABLE 2 | Average domain size of $LaCoO_3$ for fresh calcined samples and for catalysts after reaction.

Catalyst	Fresh calcined samples		Catalysts after reaction			
	$LaCoO_3$ (01-084-0848)		Co^0 (00-015-0806)		$La(OH)_3$ (00-036-1481)	
	2·θ (°)	*t*(nm)	2·θ (°)	*t*(nm)	2·θ (°)	*t*(nm)
NH4–9	47.456	45	44.077	27	39.346	16
NH4–9-E	47.586	45	44.269	37	39.533	16
NH4–11	47.483	50	44.124	22	39.360	16
NH4–11-E	47.490	37	44.321	27	39.579	16
Na-11	47.465	58	44.338	25	39.610	16
Na-11-E	47.494	54	44.122	22	39.365	14

Activity Tests Results

Conversion of methane with high selectivity to CO and H_2 can be obtained at 900°C over activated samples (under 44.4 mL_N/min flow of 10% H_2–90%N_2 for 30 min). The catalytic behavior evolves differently with time on stream depending on the type of sample (**Figure 6**). The catalysts NH4–11 and NH4–9 are the most active, selective, and stable for syngas production by CPOM along 6 h of reaction, with methane conversions and syngas selectivities in the thermodynamic equilibrium (York, 2003). They are followed in catalytic efficiency by the catalysts NH4–11-E and NH4–9-E, for which an induction period of around 5 h is observed. This induction period is explained by the progressive reduction of

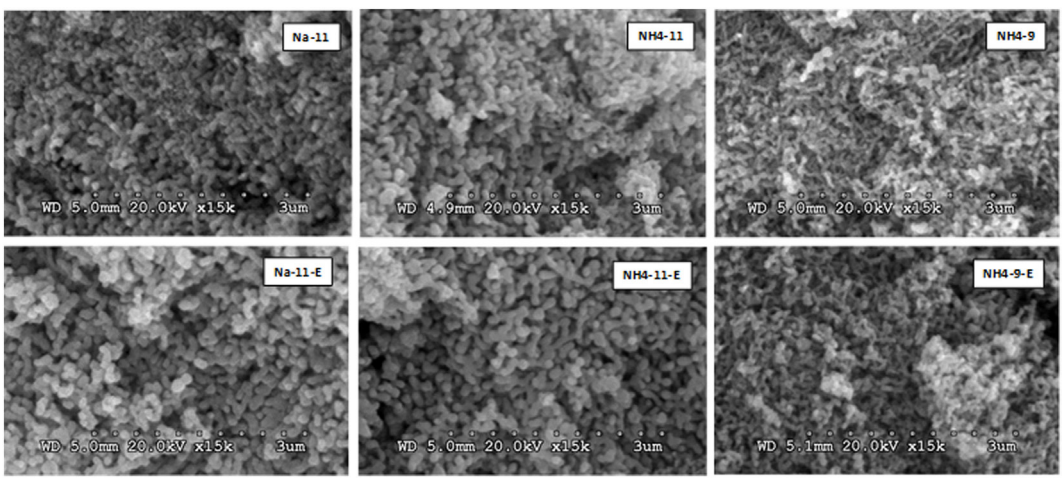

FIGURE 4 | Scanning electron microscopy micrographs of fresh calcined samples.

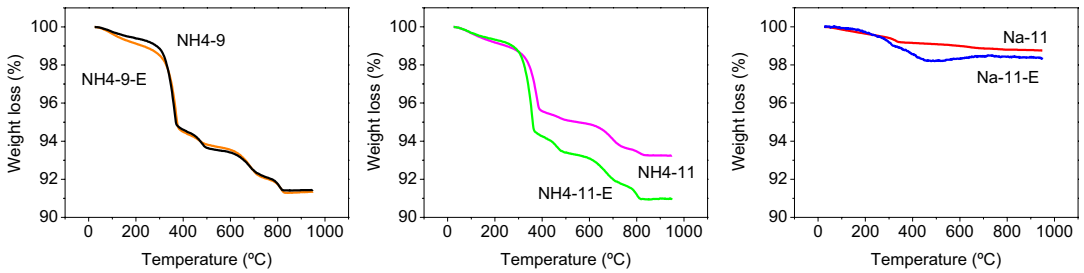

FIGURE 5 | Thermogravimetric analysis profiles of fresh calcined samples.

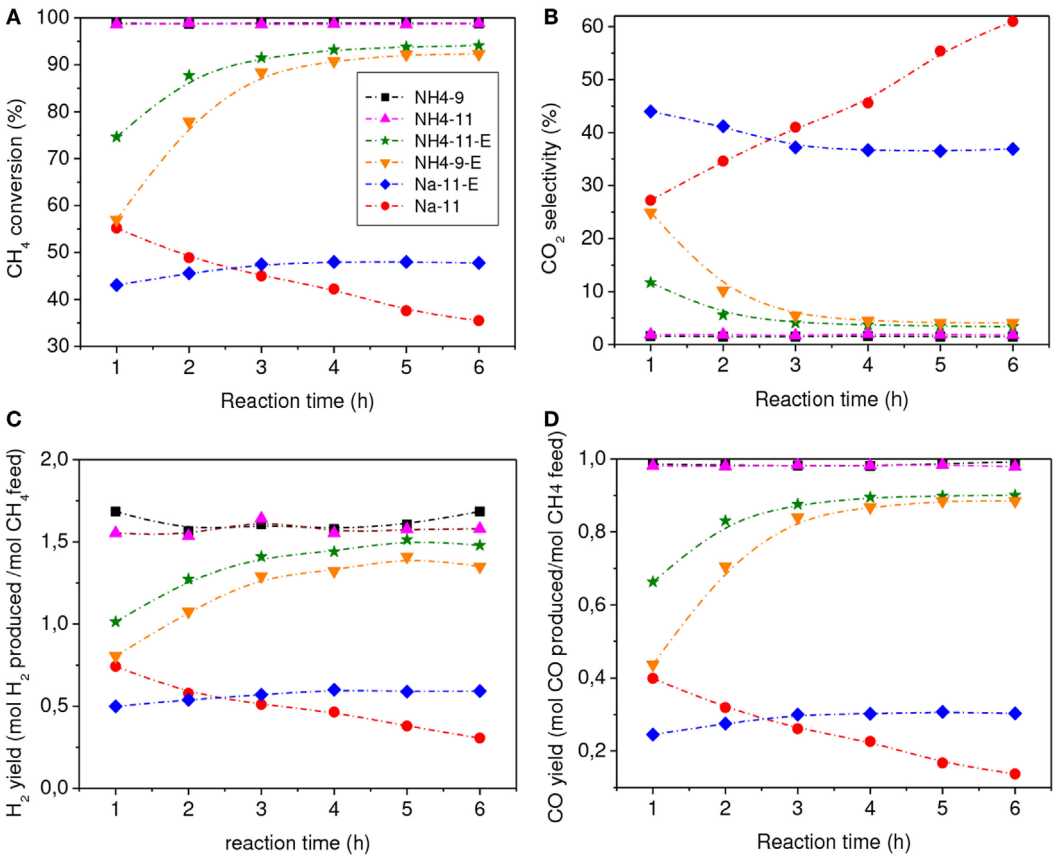

FIGURE 6 | Activity parameters of catalysts for partial oxidation of methane to syngas [900°C, 36,600 $mL_N/h \cdot g$, 40% CH_4, 20% O_2, and 40% N_2 (molar)]. **(A)** CH_4 conversion, % **(B)** CO_2 selectivity, % **(C)** H_2 yield, and **(D)** CO yield.

surface cobalt oxide to metallic cobalt under reaction conditions (Navarro et al., 2007).

Finally, the less active catalysts are those prepared using sodium hydroxide as precipitant (Na-11-E and Na-11). The catalyst Na-11-E shows a quite stable catalytic behavior in the whole reaction time. On the contrary, the catalytic performance of catalyst Na-11 changes with time on stream and an increase in the selectivity to CO_2 is observed (**Figure 6B**). This is likely due to the progressive reoxidation of the active metallic Co (Cimino et al., 2005), to cobalt oxide which is active for methane combustion. Indeed, under CPOM reaction conditions, CH_4 conversion progressively decreases from 55 to 35% and CO_2 selectivity increases from 27 to 61% during the first 6 h of reaction.

After 6 h of reaction, CH_4 conversion (**Figure 6A**) and syngas yield (**Figures 6C,D**) show the following trend: NH4–9 > NH4–11 > NH4–11-E > NH4–9-E > Na-11-E > Na-11. For the catalysts prepared using ammonium hydroxide as precipitant,

TABLE 3 | Binding energies of La3d5/2, Co2p3/2, O1s, and C1s core levels and Co/La, Co/(Co + La), CO_3^{2-}/La surface ratios for catalysts after reaction.

Catalyst	$La3d_{5/2}$	$Co2p_{3/2}$	O1s	C1s	Co/La at	Co/(Co + La)	CO_3^{2-}/La
Na-11-E	835.0	779.9	531.2	289.5	0.207	0.517	0.772
Na-11	834.9	780.0	531.1	289.7	0.171	0.534	0.670
NH4–11	835.1	780.1	531.2	289.7	0.294	0.463	0.652
NH4–11-E	835.0	779.9	531.2	289.6	0.167	0.398	0.520
NH4–9-E	834.9	779.9	531.2	289.4	0.776	0.437	0.521
NH4–9	835.1	780.0	531.2	289.7	0.130	0.419	0.499

the addition of CTAB to the synthesis medium has a detrimental effect on the catalytic performance, which is explained by a collapse of the pores created by endotemplating during the calcination and/or during the activation and reaction stages (Zou et al., 2008).

At the reaction temperature, the ratio H_2/CO in the thermodynamic equilibrium is 2. For the most active catalysts for CPOM to syngas, those prepared using ammonium hydroxide as precipitant, the ratios H_2/CO after 6 h of reaction are between 1.53 (NH4–9-E) and 1.70 (NH4–9), somewhat lower than the thermodynamic value. This is due to the coexistence of other parallel reaction pathways that are favored at such high reaction temperatures, such as the Reverse Water Gas Shift reaction (RWGS, $CO_2 + H_2 \leftrightarrows CO + H_2O$) and Reverse Boudouard reaction ($CO_2 + C \leftrightarrows 2CO$). The latter reaction enhances the formation of CO, while RWGS reaction favors CO formation and hinders H_2 production (Ozdemir et al., 2010). Both reactions therefore would decrease the H_2/CO ratio.

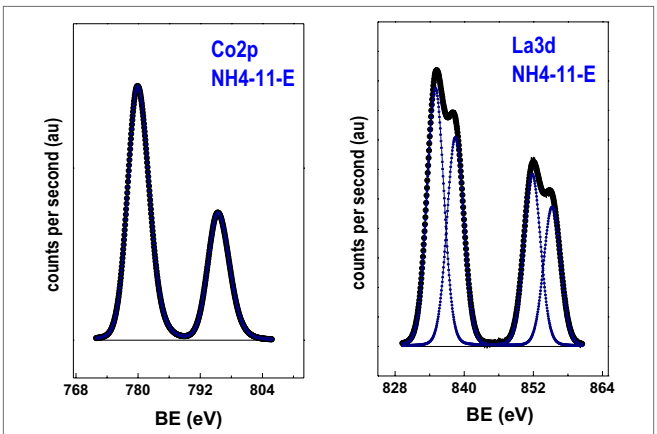

FIGURE 7 | Co2p and La3d X-ray photoelectron spectroscopy spectra of spent NH4–11-E catalyst after catalytic partial oxidation of methane reaction.

Characterization of Catalysts After Reaction

The structural composition of the catalysts after reaction has been analyzed by XRD. The diffraction profiles are shown in **Figure 3**. The only crystalline phases found in all the samples are Co^0 (PDF card 00-015-0806) and $La(OH)_3$ (PDF card 00-036-1481). The formation of these new crystalline phases are the result of the reduction of $LaCoO_3/Co_3O_4$ and other phases found in the calcined catalysts precursors both during the catalyst activation and the reaction stage. Hydroxylation of lanthanum oxide by water is responsible for the formation of $La(OH)_3$. The average domain size of metallic cobalt and lanthanum hydroxide, as determined by the Scherrer equation, are shown in **Table 2**. The mean size of Co^0 crystallites varies between 22 and 37 nm, for Na-11-E catalyst and for NH4–9-E, respectively. In the case of $La(OH)_3$, the average crystallite size changes between 14 nm (for Na-11-E) and 16 nm (for NH4–9). The introduction of CTAB decreased the average crystallite size of $La(OH)_3$. These results indicate that there is not any clear correlation between the average crystallite size of lanthanum cobaltite in fresh calcined samples and the mean crystallite sizes of crystalline phases existing in catalysts [Co^0 and $La(OH)_3$].

The surface composition of catalysts after reaction has been determined by XPS. Obtained BE corresponding to Co2p3/2, La3d5/2, O1s, and C1s levels and Co/(Co + La) ratios are reported in **Table 3**. X-ray photoelectron spectra for Co2p and La3d core levels are shown in **Figure 7** for the catalyst NH4–11-E, by way of example. The absence of a satellite peak in the Co2p spectra indicates that cobalt phase is as Co^{3+}. The C1s spectra show two components, one at 284.8 eV due to adventitious carbon contamination and another around 289.6 eV due to carbonates. Indeed, the presence of carbonate at the surface of lanthanum oxide is usual, due to the basic character of lanthana that favors the adsorption of CO_2 and formation of very stable surface carbonates (Villoria et al., 2011; Brackmann et al., 2014). For quantitative calculations only this last contribution has been considered.

In all samples, the La 3d level was characterized by a double peak for each spin–orbit component, attributed either to energy loss phenomena ("shake-up" satellites) induced by intense O 2p–La 4f charge events or to the existence of a mixing of electronic configurations (Villoria et al., 2011). The La 3d core level of catalysts after reaction showed a main component of the La 3d5/2 core level at BE of 834.9–835.1 eV, characteristic of La^{3+} in $La(OH)_3$ environment (Natile et al., 2007).

Surface Co/La ratios calculated from XPS data (**Table 3**) are substantially for the studied samples. Obtained Co/La values are lower than the nominal (1.0) for $LaCoO_3$ for all the samples. This is likely due to the segregation of La^{3+} ions on the surface, forming lanthanum carbonates and hydroxides. Regarding the Co/(Co + La) ratio, slightly higher values were found for those samples prepared using sodium hydroxide as precipitant (Na-11-E and Na-11).

The characterization of carbon deposits over the spent catalysts was carried out by Raman spectroscopy. For each catalyst, at least three Raman spectra were registered in different areas to ensure that chemical composition is homogeneous. All the Raman spectra exhibited two bands indicative of two types of carbon deposited on the catalysts: the G (graphitic) peak around 1,580/cm and the D (disordered) peak around 1,350/cm that could be attributed to the formation of carbon nanoparticles, amorphous carbon, or defective filamentous carbon. For all the spent catalysts, the intensity of the G band is higher than the intensity of the D band. In CPOM to syngas, carbon deposition is mainly produced by two different reactions: methane decomposition [$CH_4 \leftrightarrows C_{(s)} + 2H_2$; $\Delta H^0 = 75$ kJ/mol] and Boudouard reaction [$2CO \leftrightarrows C_{(s)} + CO_2$; $\Delta H^0 = -172$ kJ/mol]. However, only methane decomposition occurs at temperatures higher than 820°C (Wang et al., 1996; Ozdemir et al., 2010). Thus, under our experimental conditions we attribute carbon deposition solely to methane decomposition.

Taking into consideration the catalytic results obtained here, it can be concluded that the precipitant agent has a major influence over the catalytic behavior of $LaCoO_3$-derived catalysts for hydrogen production by partial oxidation of methane. The higher activity and selectivity obtained for the catalysts prepared using NH_4OH as precipitating agent (in comparison to NaOH) is explained by the way the cation $\left(NH_4^+\right)$ surrounds the precipitate. According to literature (Tang et al., 2009), the spatial configuration of ammonium cation decreases the grain size, which is observed at micrometer level by SEM, producing aggregates of smaller size and higher ssa and porosity. The precipitating agent also has an influence over lanthanum cobaltite crystalline domain, which is smaller for those samples precipitated with ammonium hydroxide. A semi quantitative way to represent the amount of cobalt atoms per gram of catalyst exposed at the catalyst surface, is the use of the parameter: surface atomic ratio Co/(Co + La) (XPS) multiplied by the ssa (BET). A higher yield to syngas by CPOM has been found for those catalysts with a higher surface exposure of cobalt atoms per unit of mass of catalyst (see **Figure 8**). The large values obtained for catalysts NH4–11 and NH4–11-E in contrast to Na-11 and Na-11-E indicates that the precipitating agent plays a key role on the active phase dispersion, directing the porosity and the grain size of lanthanum cobaltite.

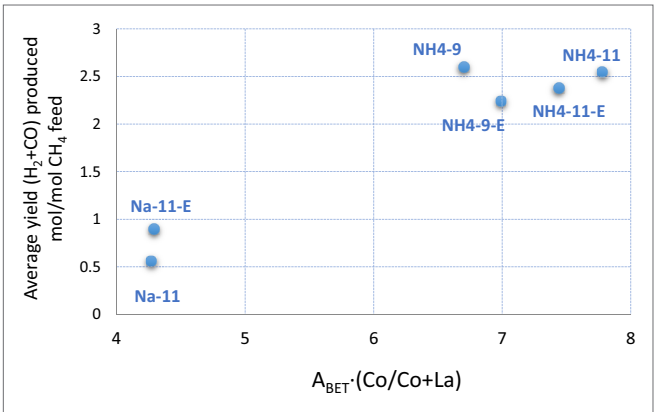

FIGURE 8 | Correlation between A_{BET}·[Co/(Co + La)] and yield to syngas by catalytic partial oxidation of methane (CPOM) for the catalysts derived from $LaCoO_3$ precursors.

CONCLUSION

In summary, a series of $LaCoO_3$ perovskites were prepared by microwave-assisted hydrothermal coprecipitation and some of them resulted in efficient catalysts for syngas production by CPOM. The XRD results confirmed the formation of the rhombohedral perovskite phase of $LaCoO_3$ for all the samples, and this was the only phase for the samples prepared using sodium hydroxide as precipitant. Textural data show that microwave-assisted hydrothermal coprecipitation leads to samples with relatively high ssa and porosity. The best catalytic performance was found for catalysts prepared using ammonium hydroxide as precipitant and without adding CTAB as endotemplate. The use of sodium hydroxide as precipitant lead to the formation of larger $LaCoO_3$ crystalline domains and grains. This leads to lower ssa, therefore decreasing the dispersion of the active phase in the catalyst. The use of ammonium hydroxide as precipitant hinders the growth of the crystal grains due to the spatial configuration of NH_4^+ cations. In this way, an increase in the porosity and in the surface active area per unit mass of catalyst is achieved.

AUTHOR CONTRIBUTIONS

AT and CA-G elaborated the samples synthesis protocol, MS-S supervised the samples preparation, CA-G carried out the preparation of the samples, Raman spectroscopy measurements, and SEM analyses and the analysis-discussion of characterization data. HF carried out the catalytic activity tests. JF carried out the XPS analyses and their discussion. All authors contributed to discussion and interpretation of experimental data.

ACKNOWLEDGMENTS

CA-G acknowledges the scientific and technical assistance of Dr. Trunschke and all her group members during her stay at AC-FHI (Department of Inorganic Chemistry, Fritz Haber Institut, Berlin). The authors gratefully acknowledge Concepción Diaz Guerri for XRD analyses, Rosa Folgado Martínez for N_2 adsorption–desorption isotherms, and Dr. Miguel A. Peña for TGA analyses.

FUNDING

The synthesis of $LaCoO_3$ samples by microwave-assisted coprecipitation was carried out at the Inorganic Chemistry Department of Fritz Haber Institute, Max-Planck Society (AC-FHI) (Berlin) under the project "Development of a novel route to create internal porosity in perovskites using endotemplates which would have potential applications in catalysis, fuel cell technology

and sensors field" (PA1002660) supported by a Grant of CSIC/DFG (German Research Foundation) through the program "Programa de Movilidad, Ayudas a Investigadores del CSIC para realización de estancias en centros de investigación extranjeros." This work was also supported by CSIC (Spain) through the grant 201680I045.

REFERENCES

Alvarez-Galvan, M. C., de la Peña O'Shea, V. A., Arzamendi, G., Pawelec, B., Gandía, L. M., and Fierro, J. L. G. (2009). Methyl ethyl ketone combustion over La-transition metal (Cr, Co, Ni, Mn) perovskites. *Appl. Catal. B. Environ.* 92, 445–453. doi:10.1016/j.apcatb.2009.09.006

Brackmann, R., Perez, C. A., and Schmal, M. (2014). $LaCoO_3$ perovskite on ceramic monoliths – pre and post reaction analyzes of the partial oxidation of methane. *Int. J. Hydrogen Energy* 39, 13991–14007. doi:10.1016/j.ijhydene.2014.07.027

Carreon, M., and Guliants, V. (2005). Ordered meso- and macroporous binary and mixed metal oxides. *Eur. J. Inorg. Chem.* 2005, 27–43. doi:10.1002/ejic.200500137

Cimino, S., Landi, G., Lisi, L., and Russo, G. (2005). Development of a dual functional structured catalyst for partial oxidation of methane to syngas. *Catal. Today* 105, 718–723. doi:10.1016/j.cattod.2005.06.058

Galal, A., Atta, N., and Ali, S. (2011). Optimization of the synthesis conditions for LaNiO3 catalyst by microwave assisted citrate method for hydrogen production. *Appl. Catal. A. Gen.* 409, 202–208. doi:10.1016/j.apcata.2011.10.005

Hayakawa, T., Andersen, A., Shimizu, M., Suzuki, K., and Takehira, K. (1993). Partial oxidation of methane to synthesis gas over some titanates based perovskite oxides. *Catal. Lett.* 22, 307–317. doi:10.1007/BF00807238

He, X., and Antonelli, D. (2002). Recent advances in synthesis and applications of transition metal containing mesoporous molecular sieves. *Angew. Chem. Int. Ed. Engl.* 41, 214–229. doi:10.1002/1521-3773(20020118)41:2<214::AID-ANIE214>3.0.CO;2-D

Hellgardt, K., and Chadwick, D. (1998). Effect of pH of precipitation on the preparation of high surface area aluminas from nitrate solutions. *Ind. Eng. Chem. Res.* 37, 405–411. doi:10.1021/ie970591a

Hu, J., Liu, Q., Shi, L., Shi, Z., and Huang, H. (2017). Silver decorated $LaMnO_3$ nanorod/graphene composite electrocatalysts as reversible metal-air battery electrodes. *Appl. Surf. Sci.* 402, 61–69. doi:10.1016/j.apsusc.2017.01.060

Ino, E., Shimizu, K., and Yamate, T. (1976). Studies on thermal decomposition process of lanthanum hydroxide. *J. Soc. Mater. Sci. Jpn.* 25, 1165–1168. doi:10.2472/jsms.25.1165

Kresge, C. T., Leonowicz, M. E., Roth, W. J., Vartuli, J. C., and Beck, J. S. (1992). Ordered mesoporous molecular sieves synthesized by a liquid-crystal template mechanism. *Nature* 359, 710–712. doi:10.1038/359710a0

Massué, C., Huang, X., Tarasov, A., Ranjan, C., Cap, S., and Schlögl, R. (2017). Microwave-assisted synthesis of stable and highly active Ir oxohydroxides for electrochemical oxidation of water. *ChemSusChem* 10, 1958–1968. doi:10.1002/cssc.201601864

Mota, N., Alvarez Galván, M. C., Navarro, R. M., Al Zahrani, S. M., Goguet, A., Daly, H., et al. (2012). Insights on the role of Ru substitution in the properties of $LaCoO_3$-based oxides as catalysts precursors for the oxidative reforming of diesel fuel. *Appl. Catal. B. Environ.* 113, 271–280. doi:10.1016/j.apcatb.2011.11.047

Natile, M., Ugel, E., Maccato, C., and Glisenti, A. (2007). $LaCoO_3$: effect of synthesis conditions on properties and reactivity. *Appl. Catal. B. Environ.* 72, 351–362. doi:10.1016/j.apcatb.2006.11.011

Navarro, R. M., Alvarez-Galvan, M. C., Villoria, J. A., Gonzalez-Jimenez, I. D., Rosa, F., and Fierro, J. L. G. (2007). Effect of Ru on $LaCoO_3$ perovskite-derived catalyst properties tested in oxidative reforming of diesel. *Appl. Catal. B. Environ.* 73, 247–258. doi:10.1016/j.apcatb.2006.12.013

Ozdemir, H., Özdemir, H., Faruk Öksüzömer, M. A., and Ali Gürkaynak, M. (2010). Preparation and characterization of Ni based catalysts for the catalytic partial oxidation of methane: effect of support basicity on H_2/CO ratio and carbon deposition. *Int. J. Hydrogen Energy* 35, 12147–12160. doi:10.1016/j.ijhydene.2010.08.091

Pal, N., and Bhaumik, A. (2013). Soft templating strategies for the synthesis of mesoporous materials: inorganic, organic–inorganic hybrid and purely organic solids. *Adv. Colloid Interface Sci.* 189, 21–41. doi:10.1016/j.cis.2012.12.002

Rao, K. J., Vaidhyanathan, B., Ganguli, M., and Ramakrishnan, P. A. (1999). Synthesis of inorganic solids using microwaves. *Chem. Mater.* 11, 882–895. doi:10.1021/cm9803859

Roseno, K. T. C., Brackmann, R., da Silva, M. A., and Schmal, M. (2016). Investigation of $LaCoO_3$, $LaFeO_3$ and $LaCo_{0.5}Fe_{0.5}O_3$ perovskites as catalyst precursors for syngas production by partial oxidation of methane. *Int. J. Hydrogen Energy* 41, 18178–18192. doi:10.1016/j.ijhydene.2016.07.207

Schuth, F. (2001). Non-siliceous mesostructured and mesoporous materialsâ. *Chem. Mater.* 13, 3184–3195. doi:10.1021/cm011030j

Schüth, F. (2003). Endo- and exotemplating to create high-surface-area inorganic materials. *Angew. Chem. Int. Ed. Engl.* 42, 3604–3622. doi:10.1002/anie.200300593

Singha, R., Shukla, A., Yadav, A., Sivakumar Konathala, L. N., and Bal, R. (2017). Effect of metal-support interaction on activity and stability of Ni-CeO_2 catalyst for partial oxidation of methane. *Appl. Catal. B. Environ.* 202, 473–488. doi:10.1016/j.apcatb.2016.09.060

Soboleva, T., Zhao, X., Malek, K., Xie, Z., Navessin, T., and Holdcroft, S. (2010). On the micro-, meso-, and macroporous structures of polymer electrolyte membrane fuel cell catalyst layers. *ACS Appl. Mater. Interfaces* 2, 375–384. doi:10.1021/am900600y

Soler-Illia, G., Sanchez, C., Lebeau, B., and Patarin, J. (2002). Chemical strategies to design textured materials: from microporous and mesoporous oxides to nanonetworks and hierarchical structures. *Chem. Rev.* 102, 4093–4138. doi:10.1021/cr0200062

Stathopoulos, V., Belessi, V., and Ladavos, A. (2001). Samarium based high surface area perovskite type oxides SmFe1-xAlxO3 (X=0.00, 0.50, 0.95). Part I, synthesis and characterization of materials. *React. Kinet. Catal. Lett.* 72, 43–48. doi:10.1023/A:1010524312637

Taguchi, A., and Schüth, F. (2005). Ordered mesoporous materials in catalysis. *Microporous Mesoporous Mater.* 77, 1–45. doi:10.1016/j.micromeso.2004.06.030

Tang, J.-L., Zhu, M.-K., Chen, C., Hou, Y.-D., Wang, H., and Yan, H. (2009). Perovskite $Pb(Sc_{1/2}Nb_{1/2})O_3$ nanopowders synthesized by surfactant-modulated precipitation. *J. Nanopart. Res.* 11, 355–363. doi:10.1007/s11051-008-9393-0

Toniolo, F., Magalhães, R. N. S. H., Perez, C. A. C., and Schmal, M. (2012). Structural investigation of $LaCoO_3$ and $LaCoCuO_3$ perovskite-type oxides and the effect of Cu on coke deposition in the partial oxidation of methane. *Appl. Catal. B. Environ.* 117, 156–166. doi:10.1016/j.apcatb.2012.01.009

Villoria, J. A., Alvarez Galvan, M. C., Al Zahrani, S. M., Palmisano, P., Specchia, S., Specchia, V., et al. (2011). Oxidative reforming of diesel fuel over $LaCoO_3$ perovskite derived catalysts: influence of perovskite synthesis method on catalyst properties and performance. *Appl. Catal. B Environ.* 105, 276–288. doi:10.1016/j.apcatb.2011.04.010

Wang, H. Y., and Ruckenstein, E. (2001). Partial oxidation of methane to synthesis gas over alkaline earth metal oxide supported cobalt catalysts. *J. Catal.* 199, 309–317. doi:10.1006/jcat.2001.3190

Wang, S., Lu, G. Q., and Millar, G. (1996). Carbon dioxide reforming of methane to produce synthesis gas over metal-supported catalysts: state of the art. *Energy Fuels* 10, 896–904. doi:10.1021/ef950227t

Xintong, P., Yang, G., Yuting, Z., Bingbing, Xu, and Fei, Qi. (2016). $LaCoO_3$ perovskite oxide activation of peroxymonosulfate for aqueous 2-phenyl-5-sulfobenzimidazole degradation: effect of synthetic method and the reaction mechanism. *Chem. Eng. J.* 304, 897–907. doi:10.1016/j.cej.2016.07.027

York, A. P. E. (2003). Brief overview of the partial oxidation of methane to synthesis gas. *Top. Catal.* 22, 345–358. doi:10.1023/A:1023552709642

Zavyalova, U., Girgsdies, F., Korup, O., Horn, R., and Schlögl, R. (2009). Microwave-assisted self-propagating combustion synthesis for uniform deposition of metal nanoparticles on ceramic monoliths. *J. Phys. Chem.C.* 113, 17493–17501. doi:10.1021/jp905692g

Zhao, C., Wang, W., Yu, Z., Zhang, H., Wang, A., and Yang, Y. (2010). Nano-$CaCO_3$ as template for preparation of disordered large mesoporous carbon with hierarchical porosities. *J. Mater. Chem.* 20, 976–980. doi:10.1039/B911913B

Zhu, J., Rahuman, M. S. M. M., van Ommen, J. G., and Lefferts, L. (2004). Dual catalyst bed concept for catalytic partial oxidation of methane to synthesis gas. *Appl. Catal. A. Gen.* 259, 95–100. doi:10.1016/j.apcata.2003.09.022

Zou, Z.-Q., Meng, M., Luo, J.-Y., Zha, Y.-Q., Xie, Y.-N., Hu, T.-D., et al. (2006). A novel mesoporous oxidation catalyst La-Co-Zr-O prepared by using nonionic and cationic surfactants as co-templates. *J. Mol. Catal. A. Chem.* 249, 240–245. doi:10.1016/j.molcata.2006.01.010

Zou, Z.-Q., Meng, M., Zha, Y.-Q., and Liu, Y. (2008). Dual templates assisted preparation and characterization of highly thermostable multicomponent mesoporous material La–Ce–Co–Zr–O used for low-temperature CO oxidation. *J. Sci. Mater.* 43, 1958–1965. doi:10.1007/s10853-008-2460-1

Conflict of Interest Statement: The authors declare that the research was conducted in the absence of any commercial or financial relationships that could be construed as a potential conflict of interest.